Dalton Transactions

Accepted Manuscript

This article can be cited before page numbers have been issued, to do this please use: S. K. Verma, P. Kumari, S. N. Ansari, M. O. Ansari, D. Deori and S. M. Mobin, *Dalton Trans.*, 2018, DOI: 10.1039/C8DT02778A.

ROYAL SOCIETY OF CHEMISTRY

rsc.li/dalton

Dalton Transactions
View Article Online
DOI: 10.1039/C8DT02778A

Journal Name

COMMUNICATION

A novel mesoionic carbene based highly fluorescent Pd(II) complex as an endoplasmic reticulum tracker in live cells

Received 00th January 20xx,
Accepted 00th January 20xx

DOI: 10.1039/x0xx00000x

www.rsc.org/

Sanjay K. Verma,[a] Pratibha Kumari,[b] Shagufi Naz Ansari,[a] Mohd Ovais Ansari,[a] Dondinath Deori[a] and Shaikh M. Mobin*[a,b,c]

A recent study advocates that endoplasmic reticulum (ER) dysfunction may link to critical neurotrauma and advanced tauopathy. In this regard, targeting ER warrants urgent attention for the therapeutic of neurotrauma-related neurodegeneration. Herein, we report the synthesis of a new N-heterocyclic mesoionic carbene based highly fluorescent square-planar Pd(II) complex 1, with high quantum yield (0.737). Probe 1 shows as a non-toxic probe for selectively labeling the endoplasmic reticulum in live cells.

Owing to advancement in bio-imaging techniques, the *in vivo* subcellular organelles targets and biochemical processes has gained much attention towards basic biomedical research and the development of novel clinical diagnostics.[1-3] In this regard, some organic ligand and metal complexes based probes have been explored.[4-6] Among sub-cellular organelles, Endoplasmic reticulum (ER) plays an important role in eukaryotic cells[7] for the synthesis and processing of proteins, and calcium storage.[8-9] The improper protein folding may interfere with ER functions. A recent development suggests that ER dysfunction is directly linked to many metabolic diseases, such as diabetes, obesity, insulin resistance, critical neurotrauma and advanced tauopathy.[10-12]

Design and synthesis of an appropriate chemical probe as the tool for the diagnosis and monitoring of disease as well as biomarkers are the current area of focus. Understanding the complex molecular interactions in the human physiological system had posed a challenging task to both chemists as well as biologist. Therefore, the fluorescent probes have become popular because of their low cost, sensitive nature and easy-to-operate and monitor various bioactive molecules in living systems for both *in vitro* as well as *in vivo* studies. To understand desired selectivity towards selective organelles, the recognition site of a fluorescent probe is designed in such a way, that maximizes the binding interactions.[13-18] Furthermore, fluorescence recovery after photobleaching (FRAP) is widely used as a powerful tool for monitoring molecular dynamics of fluorescent-tagged molecules within living cells by employing confocal microscopes (CSLMs).[19]

There exist few reports on ER tracking by employing some metal-complexes,[20] oxovanadium(IV) vitamin-B6 Schiff base complex,[21] tunicamycin-treated and organoplatinum(II) complexes containing bis(N-heterocyclic carbene)[22] but all of these lack FRAP.

So far report on Pd complexes being engaged in anti-bacterial, anti-fungal and anti-viral and more recently the anti-cancer activities with focus on tumor cell lines like breast and prostate cancer by using different ligands such as triazole, dithiocarbamate,[23] triphenylphosphines,[24] or hydrazine[25] and even curcumin, which is a well-known plant-based compound with apoptosis-inducing activity on cancer cells has been well documented. Further, better lipophilicity or solubility results in enhanced cytostatic activity of Pd(II) complexes. Only one report is available on Pt(II) complex based ER tracking, but to the best of our knowledge this is the first report on MIC based Pd(II) complex as an efficient ER tracker.[23-29]

Herein, we report the synthesis of a phenylene based MIC ligand forming Pd(II) complex and their biological evaluation which by large has been ignored till date.

Pd(II) complex **1** was synthesized by the Cu(I) catalyzed click reaction of 4-ethynyl toluene and sodium azide in the presence of sodium ascorbate and copper sulfate in *tert*-butanol and water mixture, then the resulted product was converted to its triazolium iodide salt. This triazolium salt on reaction with $PdCl_2$ in the presence of base resulted in the formation of the complex **1** (Scheme 1). The Pd(II) complex **1** is highly soluble in dichloromethane and ethyl acetate. **1** was characterized by ^{1}H, ^{13}C NMR, FTIR, mass spectroscopy and further authenticated by single crystal X-ray studies. The FTIR spectroscopy of **1** reveals the band at ~3100-3000 cm^{-1} which correspond to the presence of aromatic (C-H) stretching

[a] Discipline of Chemistry.
[b] Discipline of Biosciences and Biomedical Engineering
[c] Discipline of Metallurgy Engineering and Materials Science, Indian Institute of Technology Indore, Simrol, Khandwa Road, Indore 453552, India.
† Footnotes relating to the title and/or authors should appear here.
Electronic Supplementary Information (ESI) available: [details of any supplementary information available should be included here]. See DOI: 10.1039/x0xx00000x

View Article Online
DOI: 10.1039/C8DT02778A

vibrations.[30] The ^{1}H NMR spectrum showed the absence of triazolium signal substituted with palladium. The ^{1}H NMR spectra of the **1** shows the absence of azolium C–H proton which was observed at δ = 8.43 ppm for its parent 1-methyl-4-(p-tolyl)-1H-1,2,3-triazole compound. The resonance for the aryl C–H protons (δ = 7.37 ppm) is significantly downfield shifted compared to their corresponding resonance (δ = 7.21 ppm) in complex **1** (Figs. S1 and S3). The resonance for the C–H protons of pyridine ring were detected as multiplet at δ = 8.93, 7.78–7.80 and 7.66 ppm. Upon complex formation (**1**) the resonance for α-hydrogen atom of the pyridine ring (δ = 8.93) was more downfield shifted compared to their corresponding resonance in free pyridine (δ = 8.62).[31] The resonance for the characteristic carbene carbon atom was observed at δ = 137.1 ppm in the ^{13}C NMR spectra of complex **1** which is quite similar to corresponding compound (δ = 137.6 ppm).[32] The resonance for the α-carbon atom of the pyridine ring appeared downfield shifted: δ = 154.5 ppm (Figs. S2 and S4), compared to their corresponding resonances in free pyridine. The LC-MS spectrum of Pd(II) complex **1** having peak 697.7 corresponds to $[M+ 2Cl]^{+}$ (Fig. S5) which supports the formation of the Pd(II) complex **1**.

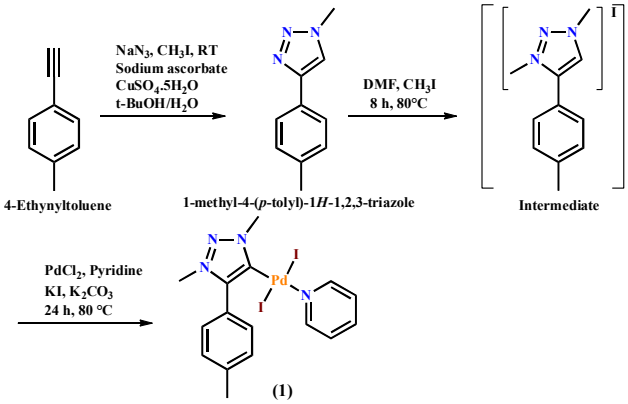

Scheme 1 Schematic representation of synthesis of Pd(II) complex **1.**

Single crystal suitable for X-ray diffraction study was obtained by slow evaporation of the dichloromethane-hexane solution of **1** at room temperature. Complex **1** that crystallizes in monoclinic $P2_1/n$ space group reveals the formation of the mononuclear **1** (Table S1). The Pd(II) atom in **1** is coordinated by a C-donor from MIC ligand and N-donor from pyridine, in a trans-fashion and remaining coordination sites are occupied by two iodide donors (Fig. 1a) forming square planar geometry around the Pd atom. The C9–Pd1–N4 bond angle is almost linear with 177.77(5)°and the Pd1–C9 (1.967(8) Å) and Pd1–N4 (2.100(6) Å) bond lengths are in the range previously described for Pd(II) MIC complexes.[33-34] The dihedral angle between the NHC plane {N1 N2 N3 C8 C9} and the phenyl ring plane {C2 C3 C4 C5 C6 C7} is found to be 43.09° (Fig. S6). The Pd–Py and triazole carbon-Pd moieties are twisted in the opposite direction, thus featuring anti-geometry of the complex **1** (Fig. 1a).

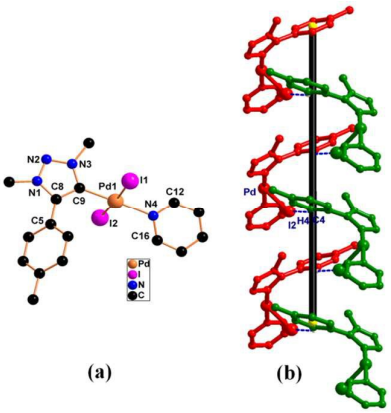

Fig. 1 (a) Perspective view of **1 (b)** Helical view of **1** via intermolecular I2...H4–C4 interactions**.**

The packing diagram of 1 reveals the presence of C–H···I interaction. The intermolecular C(4)–H(4)···I(2) interactions, 3.092 Å, involve the donor carbon atom of the phenyl group and the acceptor I(2) atom of the other molecule leading to the formation of 1D-polymeric chains (Fig. S7) resembling single-stranded *helical* structure of **1** via I2...H4–C4 interaction along b-axis (Figs. 1b and S8).

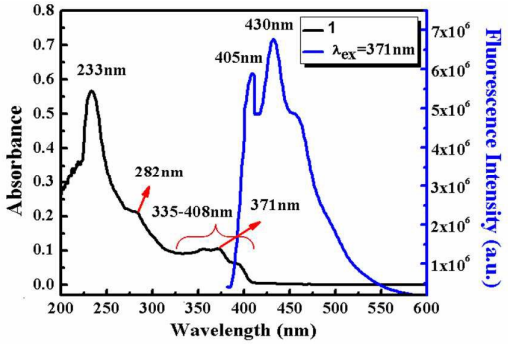

Fig. 2 UV-visible (black) and fluorescence spectrum (blue) of the complex **1** at room temperature in 10^{-4} M tetrahydrofuran solution.

The electronic absorption and emission spectra of the **1** were recorded in tetrahydrofuran solution. The absorption bands of **1** at 233, 282 and 371 nm is attributed to the π→π* (aromatic moiety) and n→π* (triazole and pyridine) transitions respectively, for ligand moiety, occurring due to the hetero-aromatic moiety (Fig. 2). The fluorescence emission data of **1** was recorded in tetrahydrofuran solution upon excitation at λ_{ex} = 371 nm. The emission spectrum of **1** exhibited the highest intensity band at 405 and 430 nm via vibronic splitting (Figure 2). Moreover, the Stokes shifts of Pd (II) complex **1** found to be 34 and 59 nm. The quantum yield of **1** was found to be very high, 0.737 (Fig. 2).

We have recorded the emission spectra of Pd(II) complex **1** in 1% DMSO with various solvents (Acetonitrile/THF/Methanol /Water) and found that the emission band splits into two partially resolved bands except in water (Fig. S9). This may be due to the strong hydrogen bonding between complex **1** and

View Article Online
DOI: 10.1039/C8DT02778A

H_2O which lock the molecule for the vibronic coupling. Fluorescence intensity of **1** was found to be trivial quenching at high pH (phosphate buffer saline containing 1% DMSO at various pH) this may be due to the formation of electron donor 1,2,3-triazole/iodine, through photo induced electron transfer (PET) under basic conditions. **1** showed slightly red shifted with decrease in pH upto 3.1 and quite stable up to pH 7.4 (Fig. 3A). Fluorescence emission of **1** was also investigated in micelles of positively charged cetyl-trimethyl-ammonium bromide (CTAB) and negatively charged sodium dodecyl sulfate (SDS) at 5.0 mM and 2.0 mM concentration respectively for mimicking the probe in the cell membranes (Fig. 3B and Fig. 3C). In addition, the fluorescence behaviors of the **1** was unaffected at studied pH range, indicating that the binding of the probe to the micelles efficiently shields the probe from the aqueous environment. These results imply that the **1** can be localized in the membrane phases rather than in the aqueous phase in the cells.

The Pd(II) complexes are known for their extraordinary photoluminescence due to the σ-donating property of the anionic carbons, which effectively raises the energy of the d-d states, diminishing their deactivating effect.[33-34] Further, the photoluminescence spectra of **1** shows two separate electronic transitions at 370 and 392 nm attributed to π*→π and π*→n transitions for ligand moiety (Fig. S10) upon excitation at 25 °C (λ_{ex} = 282 nm) as expected in such Pd(II)/Pt(II) complexes.[35-37]

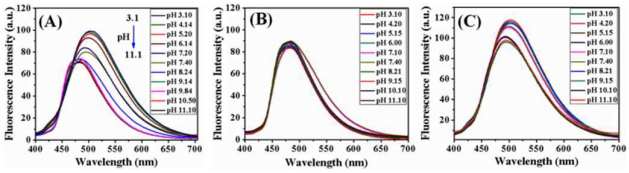

Fig. 3 (A) Fluorescence emission spectra of Pd(II) complex **1** (10 μM) at different pH {1% DMSO in PBS (Phosphate-buffered saline)} solution upon excitation at 371 nm (B) In the presence of 5.0 mM, CTAB (positively charged micelles) (C) In the presence of 2.0 mM, SDS (negatively charged micelles).

The highly fluorescent nature of **1** prompted us to explore the role of **1** in live cells as a potential candidate for cellular organelles marker. To initiate biological activities, the probe **1** was checked for it cytotoxicity on both cancerous as well as normal cells i.e. HeLa (cervical cancer cells) and HEK 293 (human embryonic kidney cells 293) cell and was found to be non-toxic at the concentration upto 180 μM for 24 h as proved by cell viability assay using MTT (Fig. S11). Further, Flow cytometry acquire superior quality fluorescence signals with an elevated spatial resolution from significant population of cells in flow.[38-40] Probe **1** labeled HeLa cells were estimated by flow cytometry (Fig. S12). Mean fluorescence intensity of huge number of cells shifted from quadrant Q3-2 (control) to Q4-3 (treated) (Fig. S12a) and subsequent shift in histogram towards higher intensity was also observed (Fig. S12b). Moreover, mean fluorescence intensity of untreated cells was as low as 62 as compared to treated cells having higher mean fluorescence intensity 2759. This indicates **1** can uniformly label enormous population of cells; which was detected in live suspension cells by flow cytometer. Rapid population-based fluorescence statistic data of flow cytometry is further supported by the pictorial images of confocal laser scanning microscope.

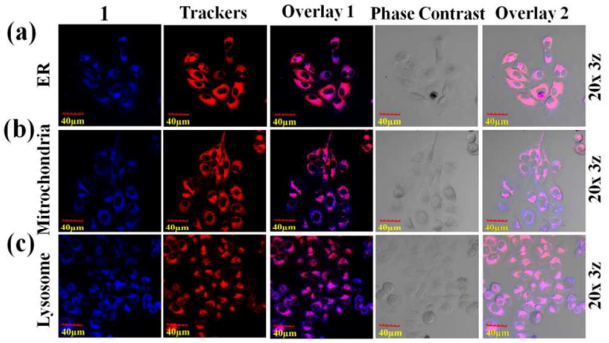

Fig. 4 HeLa cells co-labeled with 1 (100 μM) and organelle markers. (a) ER-Tracker Red for Endoplasmic Reticulum (1 μM); (b) MitoTracker Red CMXRos (80 nM) for mitochondria; (c) LysoTracker Red DND-99 (100 nM) for lysosomes. The images from left to right shows L-lyso (column 1), organelle trackers (column 2) phase contrast (column 3), and Overlay 1: overlay of the 1st and 2nd columns. Overlay 2: overlay of the 1st, 2nd and 3rd columns. Scale bar: 40 μm.

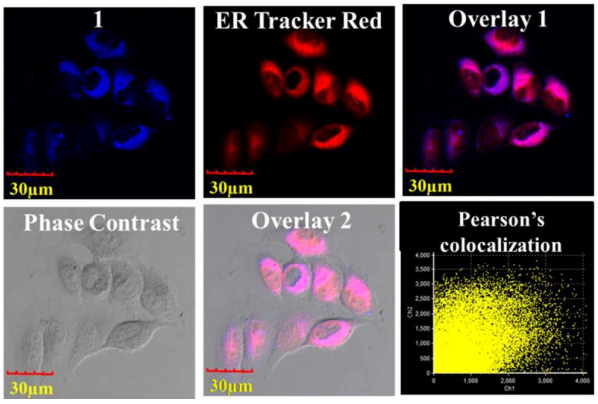

Fig. 5 ER selective imaging of living HeLa cells treated with 1. Live HeLa cells treated with 1 (100 μM) and ER-tracker Red (1 μM). The fluorescence emission of 1 (blue), ER-tracker Red (red) Colocalization of these two fluorophores is overlay 1 and 2 (pink). Pearson colocalization graph (yellow). Probe 1: λ_{ex} = 405 nm; λ_{em} = 415-470 nm; ER-Tracker Red λ_{ex} = 559 nm; λ_{em} = 580-700 nm.

To confirm the initial cellular location of probe **1**, HeLa cells treated with probe **1** and images were captured in both blue and red channel, probe is fluorescent in blue channel and non-fluorescent in red channel, hence probe **1** was excited by 405nm not by 599nm (Fig. S13). So that we performed co-localization experiments with three commercially available red fluorescent organelle trackers (ER-Tracker Red for endoplasmic

View Article Online
DOI: 10.1039/C8DT02778A

reticulum, MitoTracker Red CMXRos for mitochondria and LysoTracker Red DND99 for lysosome). The fluorescent co-localization images (pink) of **1** with those organelle trackers (Fig. 4) indicated that **1** overlapped well with ER-tracker Red with high Pearson's co-localization coefficient R_r = 0.75 (Fig. 4a and Fig. 5). However, poor co-registration effect having R_r value = 0.44, 0.49 for mitochondria and lysosome, respectively (Figure 4b and 4c). Moreover, Manders' coefficients were calculated having Manders' M1 = 0.901 and Manders' M2 = 0.679 signifying good colocalization of probe **1** (blue) and ER tracker red (red) on a per-pixel level. This demonstrates that the probe **1** is highly selective towards localization in Endoplasmic reticulum and also compatible for counter staining with LysoTracker Red and Mito Tracker Red.

The photostability plays an important role for any marker in the cell to observe long-term imaging during physiological and morphological alterations in a stipulated time. In this regard, the photostability of **1** was studied in live HeLa cells and was compared with commercially available ER-Tracker Red. Fluorescence intensity initially decreases and after 200 scans it reaches 70% due to photobleaching but gradually recover again upto 98% after 1800 scans (Fig. 6, Movies S1 and S2).

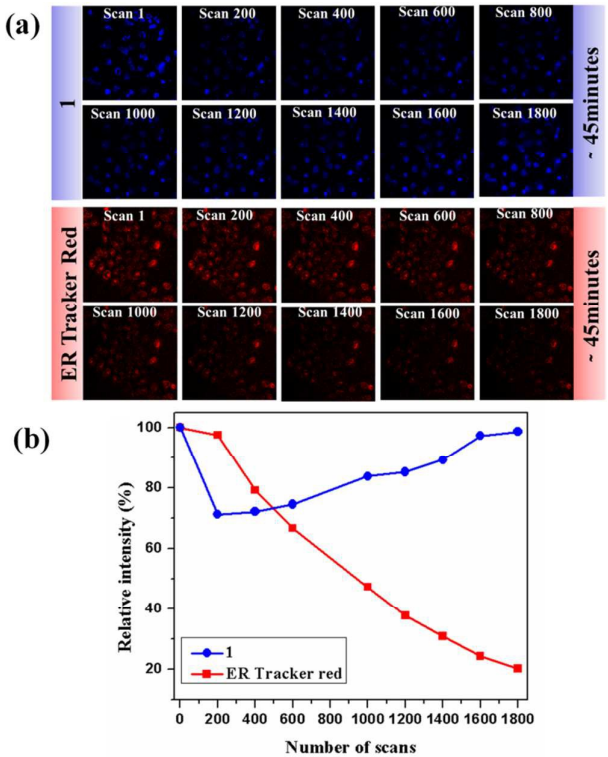

Fig. 6 Comparisons of the photostability of probe 1 and ER-Tracker Red in HeLa cell lines. (a) Confocal images of 1 (100 μM, λ_{ex} = 405nm, λ_{em} = 415–470 nm) and ER-Tracker Red (1 μM, λ_{ex} = 559 nm, λ_{em} = 580–700 nm) for photobleaching in HeLa cells. (b) Comparative Photostability Graph of ER-Tracker Red and 1.

This results the fluorescence recovery after photobleaching (FRAP) in case of **1**. This may be due to any of the following reasons (i) diffusion of soluble fluorescent probe **1** in ER membrane and (ii) due to the movement of **1** between organelles. On the contrary, the ER-Tracker Red shows very poor photostability with the intensity being reduced to 20% of the initial intensity after 1800 scans, and could not recover back during laser scanning.

3D tumor spheroids possess numerous features that mimic *in vivo* tumors such as cell-cell interaction, hypoxia cells at center and a well-oxygenated outer layer of the cells. In order to explore **1** towards 3D tumor spheroids, the fluorescence images were captured every 2μm along the *Z*-axis. **1** penetrates to a depth of ~48μm whereas ER tracker penetrates upto ~24μm depth (Fig. S14, S15 and Movie S3, Movie 4). This suggests that the compound 1 exhibited more fluorescence in deep layer cells of spheroids as compared to standard dye.

Conclusions

In conclusion, we report a rare example of the synthesis of new organometallic MIC based mononuclear Pd(II) complex **1**. The higher quantum yield and non-toxic nature of **1** make it a potential candidate for inter-cellular uptake. The fluorescence behavior of **1** was unaffected at broad pH range, indicating that the binding of the probe to the micelles efficiently shields the probe from the aqueous environment. Thus **1** specifically targets ER of live cells and plays an important role in the movement of particles between organelles due to fluorescence recovery after photobleaching (FRAP) property. **1** shows rare FRAP property as compared to so far reported Pd / Pt complexes as well as commercially available ER-Tracker Red. All these properties make **1** as a potential candidate for its commercial use.

Conflicts of interest

"There are no conflicts to declare".

Acknowledgments

Authors are grateful to the Sophisticated Instrumentation Centre (SIC), IIT Indore for providing characterization facilities. SKV is grateful to SERB for providing National Post-doctoral Fellowship, PK, SNA are thankful to MHRD, New Delhi for fellowship, MOA is thankful to IIT Indore for his internship. SMM is thankful to SERB-DST (Project No, EMR/2016/001113), New Delhi, Govt. of India and IIT Indore for financial support. This work is dedicated to Professor Dr. Dietmar Stalke on his 60th birthday.

Notes and references

Crystal data of **1**: $C_{16}H_{18}I_2N_4Pd$, *M* = 626.54, monoclinic $P2_1/n$, *Z* = 4, *T* = 293(2) K, F(000) = 1176.0, *a* = 10.7786(5) Å, *b* = 8.1520(3) Å, *c* = 23.4486(10) Å, *α* = 90°, *β* = 99.338(4)°, *γ* = 90°, *V* = 2033.06(15) Å^3, size = 0.25 × 0.23 × 0.2, Index ranges = -14 ≤ h ≤

DOI: 10.1039/C8DT02778A

13, -10 ≤ k ≤ 11, -29 ≤ l ≤ 31, Radiation = MoKα (λ = 0.71073), μ = 3.953 mm^{-1}, 2Θ range for data collection = 6 to 57.682, GOF = 1.045, Reflections collected/ Independent = 11043/4670 [R_{int} = 0.0283, R_{sigma} = 0.0267], *R* indexes [I>=2σ (I)] = R_1 = 0.0434, wR_2 = 0.1117, *R* indexes [all data] = R_1 = 0.0488, wR_2 = 0.1154, CCDC = 1573135.

1 P. Walter and D. Ron, *Science*, 2011, **334**, 1081–1086.
2 I. Kim, W. Xu and J. C. Reed, *Nature Reviews Drug Discovery*, 2008, **7**, 1013–1030.
3 L. McDonald, B. Liu, A. Taraboletti, K. Whiddon, L. P. Shriver, M. Konopka, Q. Liu and Y. Pang, *J. Mater. Chem. B*, 2016, **4**, 7902–7908.
4 S. Huang, R. Han, Q. Zhuang, L. Du, H. Jia, Y. Liu and Y. Liu, *Biosensors and Bioelectronics*, 2015, **71**, 313–321.
5 P. Kumari, S. K. Verma and S. M. Mobin, *Chem. Commun.*, 2018, **54**, 539–542.
6 A. K. Saini, V. Sharma, P. Mathur and M. M. Shaikh, *Scientific Reports*, 2016, **6**, 34807.
7 T. Zou, C.-N. Lok, Y. M. E. Fung and C.-M. Che, *Chem. Commun.*, 2013, **49**, 5423–5425.
8 H. P. Harding, Y. Zhang and D. Ron, *Nature*, 1999, **397**, 271–274.
9 J. Stevenson, E. Y. Huang and J. A. Olzmann, *Annual Review of Nutrition*, 2016, **36**, 511–542.
10 J. Matthew Meinig, L. Fu and B. R. Peterson, *Angew Chem Int Ed Engl*, 2015, **54**, 9696–9699.
11 R. J. Deshaies, *BMC Biol*, , DOI:10.1186/s12915-014-0094-0.
12 G. C. Shore, F. R. Papa and S. A. Oakes, *Curr. Opin. Cell Biol.*, 2011, **23**, 143–149.
13 C. Segarra, G. Guisado-Barrios, F. E. Hahn and E. Peris, *Organometallics*, 2014, **33**, 5077–5080.
14 C. Radloff, F. E. Hahn, T. Pape and R. Fröhlich, *Dalton Trans.*, 2009, **0**, 7215–7222.
15 C. Radloff, J. J. Weigand and F. E. Hahn, *Dalton Trans.*, 2009, **0**, 9392–9394.
16 Y. Han, L. J. Lee and H. V. Huynh, *Chem. Eur. J.*, 2010, **16**, 771–773.
17 A. Rit, T. Pape and F. E. Hahn, *J. Am. Chem. Soc.*, 2010, **132**, 4572–4573.
18 R. Maity, A. Rit, C. S. to Brinke, C. G. Daniliuc and F. E. Hahn, *Chem. Commun.*, 2013, **49**, 1011–1013.
19 Jose´ Braga, Joana M.P. Desterro and Maria Carmo-Fonseca, 2004, **15**, 4749–4760.
20 S. Banerjee, A. Dixit, R. N. Shridharan, A. A. Karande and A. R. Chakravarty, *Chem. Commun.*, 2014, **50**, 5590–5592.
21 H.-R. Kim, R. Kumar, W. Kim, J. H. Lee, M. Suh, A. Sharma, C. H. Kim, C. Kang and J. S. Kim, *Chem. Commun.*, 2016, **52**, 7134–7137.
22 T. Zou, C.-N. Lok, Y. M. E. Fung and C.-M. Che, *Chem. Commun.*, 2013, **49**, 5423–5425.
23 S. Nadeem, M. Bolte, S. Ahmad, T. Fazeelat, S. A. Tirmizi, M. K. Rauf, S. A. Sattar, S. Siddiq, A. Hameed and S. Z. Haider, *Inorganica Chimica Acta*, 2010, **363**, 3261–3269.
24 H. Khan, A. Badshah, G. Murtaz, M. Said, Z.- Rehman, C. Neuhausen, M. Todorova, B. J. Jean-Claude and I. S. Butler, *European Journal of Medicinal Chemistry*, 2011, **46**, 4071–4077.
25 S. Mukherjee, S. Chowdhury, A. P. Chattapadhyay and A. Bhattacharya, *Inorganica Chimica Acta*, 2011, **373**, 40–46.
26 A. Valentini, F. Conforti, A. Crispini, A. De Martino, R. Condello, C. Stellitano, G. Rotilio, M. Ghedini, G. Federici, S. Bernardini and D. Pucci, *J. Med. Chem.*, 2009, **52**, 484–491.
27 A. Divsalar, A. A. Saboury, H. Mansoori-Torshizi and F. Ahmad, *J. Phys. Chem. B*, 2010, **114**, 3639–3647.
28 I. Eryazici, C. N. Moorefield and G. R. Newkome, *Chem. Rev.*, 2008, **108**, 1834–1895.
29 J. Ruiz, M. D. Villa, N. Cutillas, G. López, C. de Haro, D. Bautista, V. Moreno and L. Valencia, *Inorg. Chem.*, 2008, **47**, 4490–4505.
30 M. Tavassoli, A. Landarani-Isfahani, M. Moghadam, S. Tangestaninejad, V. Mirkhani and I. Mohammadpoor-Baltork, *ACS Sustainable Chem. Eng.*, 2016, **4**, 1454–1462.
31 G. R. Fulmer, A. J. M. Miller, N. H. Sherden, H. E. Gottlieb, A. Nudelman, B. M. Stoltz, J. E. Bercaw and K. I. Goldberg, *Organometallics*, 2010, **29**, 2176–2179.
32 R. Maity, M. van der Meer and B. Sarkar, *Dalton Trans.*, 2014, **44**, 46–49.
33 W. A. Herrmann, *Angew. Chem. Int. Ed.*, 2002, **41**, 1290–1309.
34 F. E. Hahn and M. C. Jahnke, *Angewandte Chemie International Edition*, 2008, **47**, 3122–3172.
35 D. Pugh and A. A. Danopoulos, *Coordination Chemistry Reviews*, 2007, **251**, 610–641.
36 C. J. Adams, N. Fey, M. Parfitt, S. J. A. Pope and J. A. Weinstein, *Dalton Trans.*, 2007, **0**, 4446–4456.
37 S. D. Cummings and R. Eisenberg, *J. Am. Chem. Soc.*, 1996, **118**, 1949–1960.
38 D.-Y. Zhang, Y. Zheng, C.-P. Tan, J.-H. Sun, W. Zhang, L.-N. Ji and Z.-W. Mao, *ACS Appl. Mater. Interfaces*, 2017, **9**, 6761–6771.
39 W. L Godfrey, D. M Hill, J. Kilgore, G. M Buller, J. Bradford, D. R Gray, I. Clements, K. Oakleaf, J. J Salisbury, M. J Ignatius and M. Janes, *Microscopy and microanalysis : the official journal of Microscopy Society of America, Microbeam Analysis Society, Microscopical Society of Canada*, 2005, **11**, 246–247.
40 X. Chen, Y. Bi, T. Wang, P. Li, X. Yan, S. Hou, C. E. Bammert, J. Ju, K. M. Gibson, W. J. Pavan and L. Bi, *Sci Rep*, , DOI:10.1038/srep09004.

View Article Online
DOI: 10.1039/C8DT02778A

Table of contents (TOC)

A novel mesoionic carbene based highly fluorescent Pd(II) complex as a endoplasmic reticulum tracker in live cells

Sanjay K. Verma,[a] Pratibha Kumari,[b] Shagufi Naz Ansari,[a] Mohd Ovais Ansari,[a] Dondinath Deori[a] and Shaikh M. Mobin*[a,b,c]

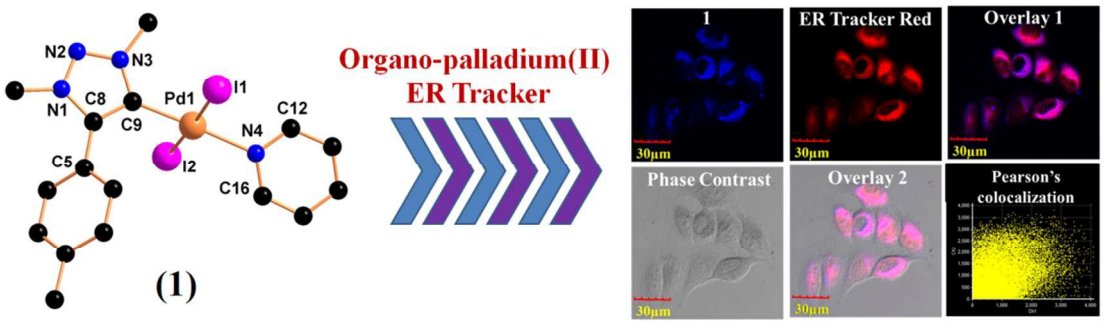

Synthesis of new organometallic MIC based mononuclear Pd(II) complex **1**, specifically target ER of live cells and plays an important role in the movement of particles between organelles due to fluorescence recovery after photobleaching (FRAP) property.